Klein et al., http://www.jcb.org/cgi/content/full/jcb.201207161/DC1

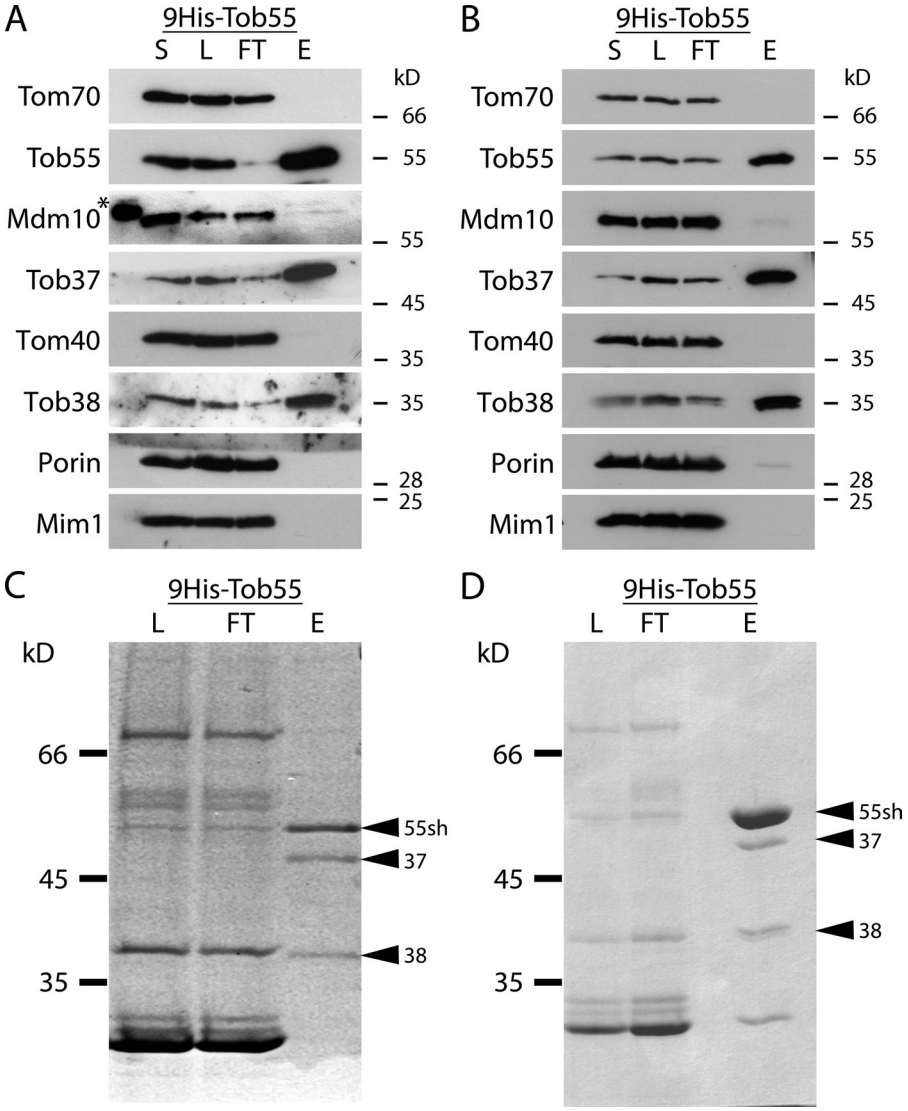

Figure S1. **TOB isolation via His-tagged Tob55.** (A–D) OMVs from cells with His-tagged Tob55 were solubilized with TX-100 (A and C) and digitonin (B and D). Proteins were isolated by Ni-NTA affinity purification and analyzed by SDS-PAGE followed by immunodecoration (A and B) and Coomassie blue staining (C and D). The calculated molecular weights for the proteins decorated are shown in A and B. The positions of molecular weight standards are shown in C and D. Solubilized OMVs before (S) and after (L) a clarifying spin. FT, flow through (proteins not bound to the Ni-NTA column); E, eluate of bound proteins; 55sh, Tob55 short isoform; 37, Tob37; 38, Tob38. The asterisk indicates nonspecific decoration of a marker protein.

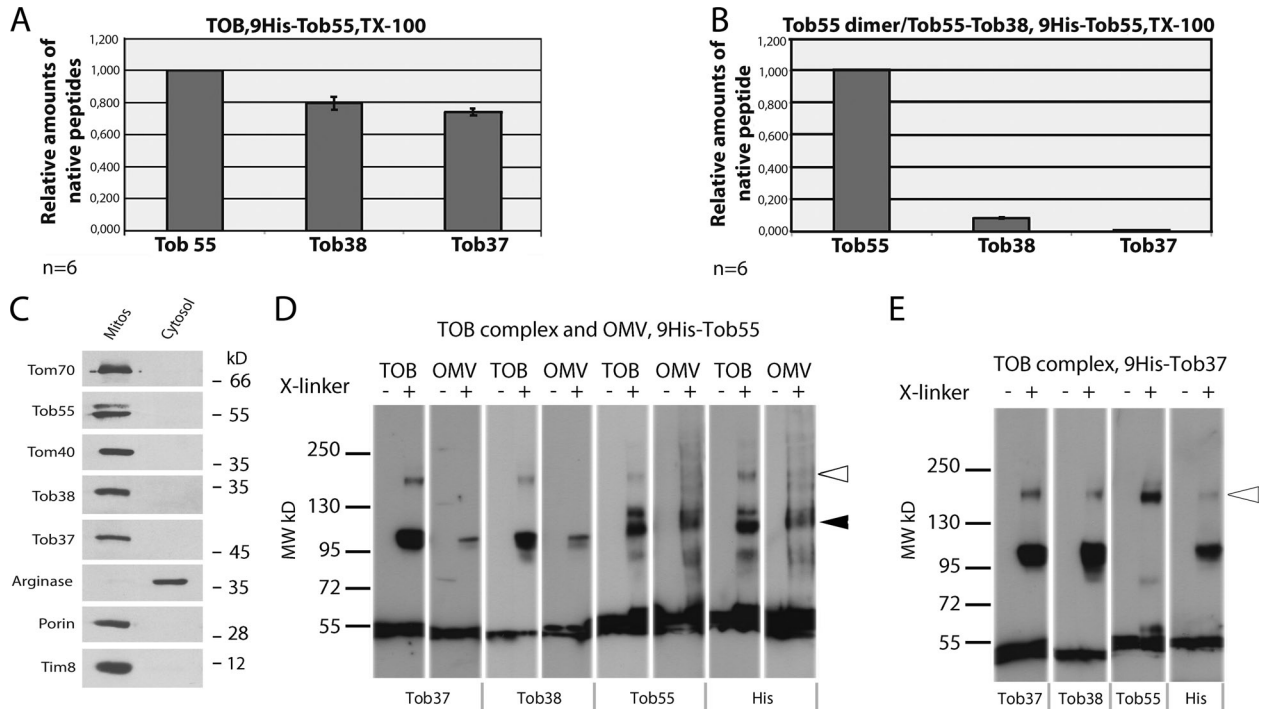

Figure S2. **TOB isolation via His-tagged Tob55 leads to copurification of Tob55 dimers.** (A and B) The TOB complex was isolated from cells expressing His_9-Tob55 using TX-100 and subjected BNGE. Proteins were stained with Coomassie blue and the bands were excised from the gel. Their composition was analyzed by IDMS. Evaluation of the data was as in Fig. 3. (C) Mitochondria and post-mitochondrial supernatant (cytosol) were analyzed by SDS-PAGE followed by immunodecoration. (D and E) The calculated molecular weights for the proteins decorated are shown in C. The positions of molecular weight standards are shown in D and E. OMVs from cells expressing His_9-Tob55 were subjected to cross-linking. Likewise, TOB complex was isolated from cells expressing His_9-Tob55 or His_9-Tob37 using digitonin and subjected to cross-linking. DSG (disuccinimidyl glutarate) was used as cross-linker. Samples were analyzed by SDS-PAGE and immunodecoration with antibodies against Tob55, Tob38, Tob37, and monoclonal His-antibody. (E) OMVs and TOB complex from cells expressing His_9-Tob55. (F) TOB complex from cells expressing His_9-Tob37. Closed arrowhead, Tob55 dimer; open arrowheads, TOB complex.

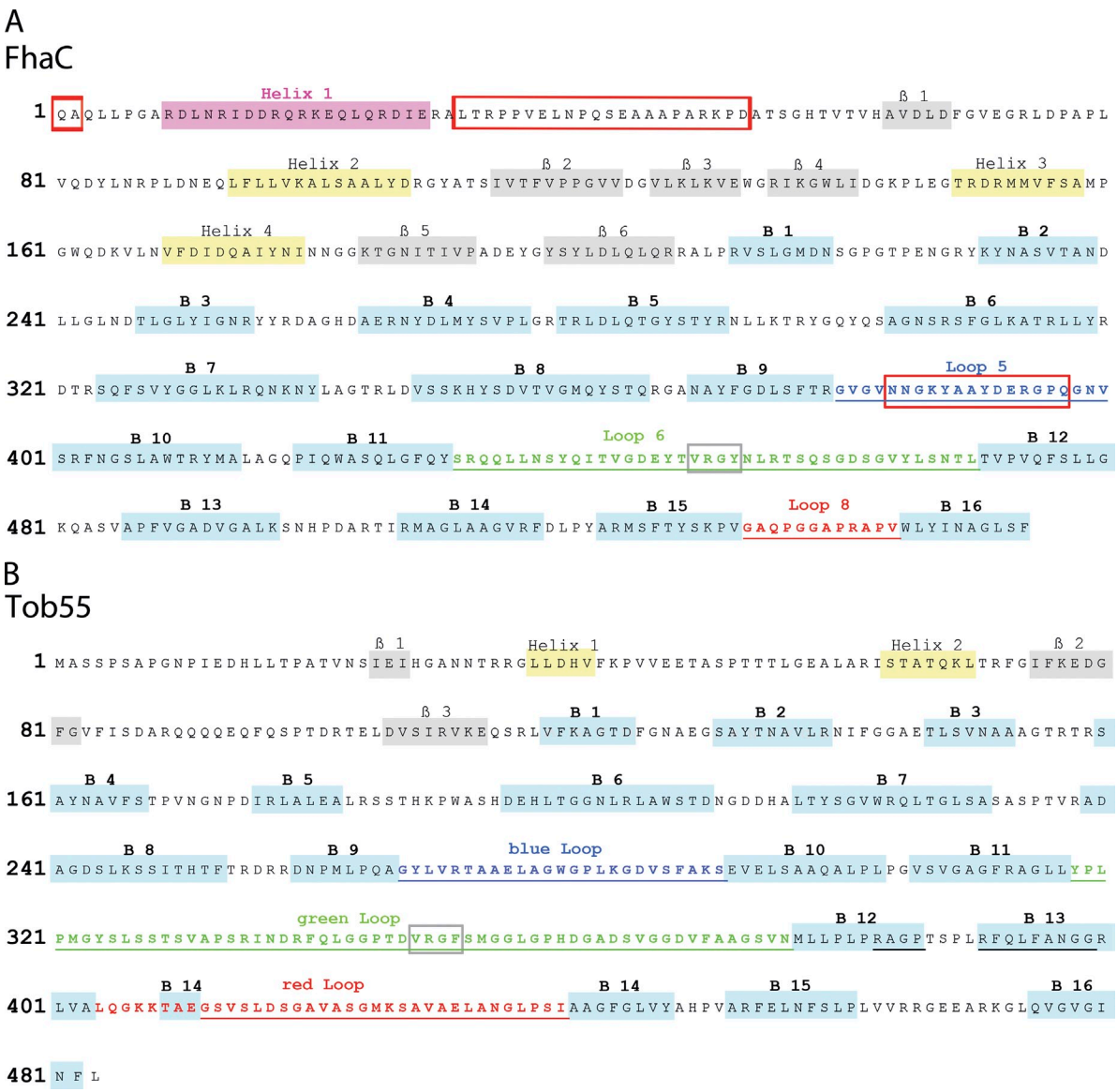

Figure S3. **Analysis of secondary structure elements of FhaC and Tob55.** (A and B) Secondary structural elements of FhaC (A) and Tob55 (B). Helices and β-strands of the N-terminal domain are presented in yellow and gray, respectively. β-Strands that are forming the β-barrel are colored in light blue. The FhaC structure does not include the first two N-terminal residues, the loop after helix 1 (residues 31–52), as well as residues 384–398 of loop 5 (framed in red). The loop that spans the interior of both β-barrels (green loop) harbors the VRGY/F tetrad (framed in gray). Amino acid residues which were not part of β-strands in the two-dimensional structure prediction of Tob55 but turned out to contribute to the β-strands in the three-dimensional modeling are underlined in black (β-strands 12–13).

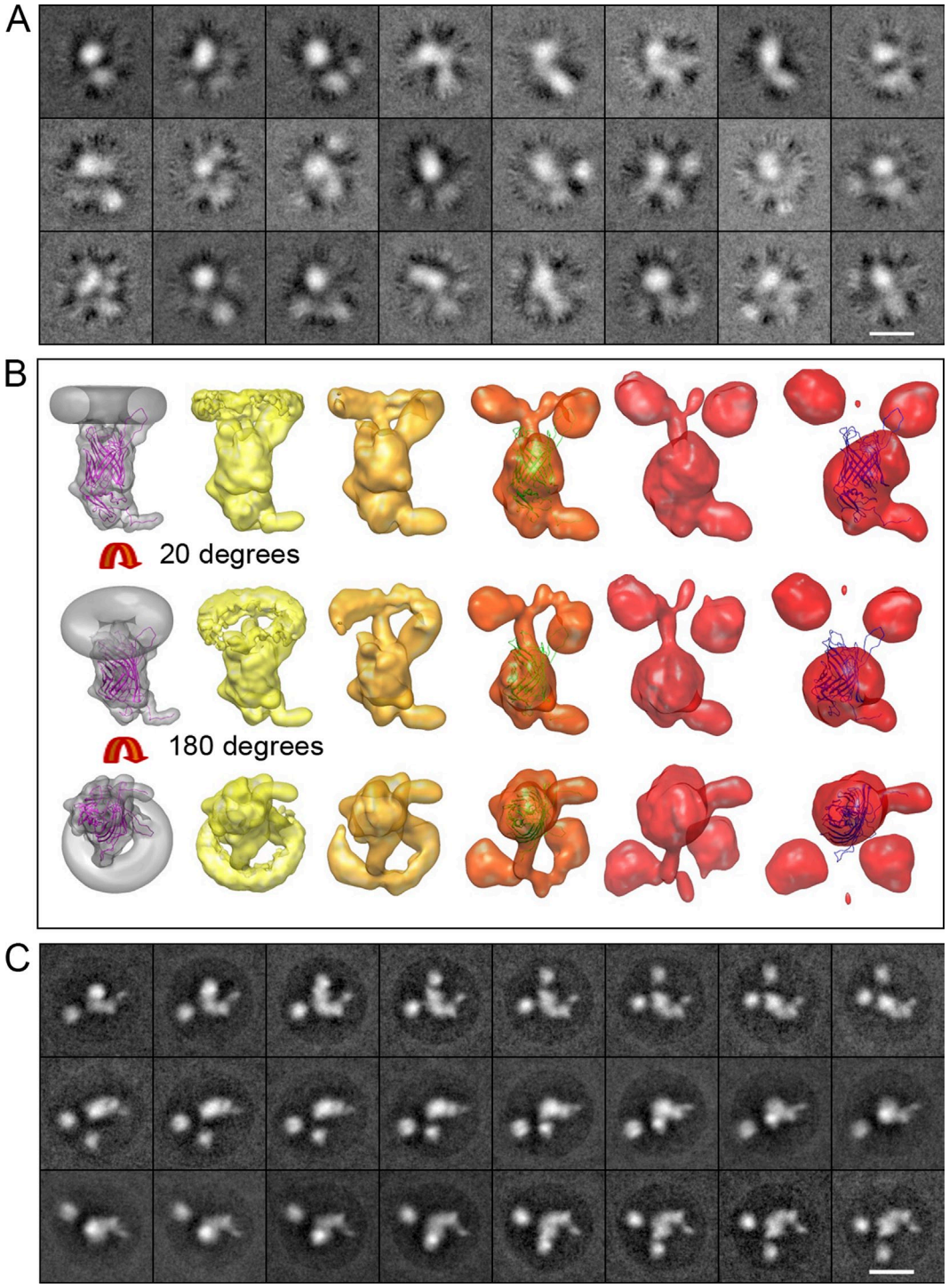

Figure S4. **Progress of the His_9-Tob37 TOB complex reconstruction TOB from model to structure and reference-free alignment of single-particle images.** (A) Subset of class averages after classification of reference-free aligned images. (B) Different orientations of the starting model (gray) and subsequent reconstructions are shown, illustrating the transformation that occurred over 20 rounds of alignment and reconstruction. (C) Averages of images matching a subset of the reference projections after the final round of alignment and reconstruction that generated the map. Bar: (A and C), 10 nm.

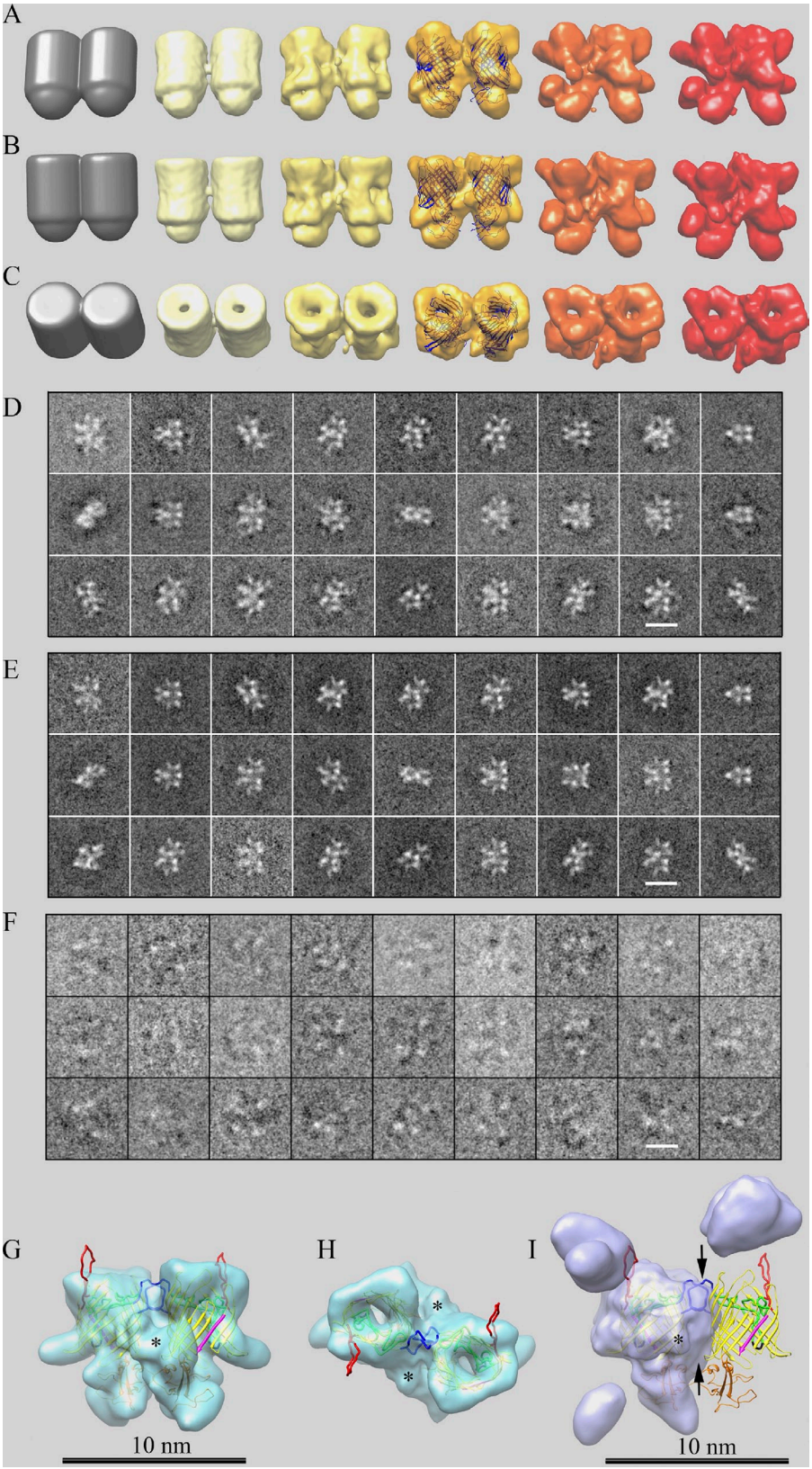

Figure S5. **Progression from cylinders to Tob55 dimers.** (A–C) Different views of the starting reference (gray) and intermediate reconstructions obtained with successive rounds of alignment (10 total). (D) A subset of the class averages obtained from classification of the final aligned images (500 classes). These class averages were aligned to the references (450 reference projections) used for the last round of alignment to determine which projection they matched. (E) Averages of the aligned images matching a particular reference projection. The images in D and E correspond to the same reference projections. This result indicates that classification was able to sort the images into classes representing specific views of the Tob55 dimer. (F) Beginning with the same starting two-cylinder reference, 7,300 images of the buffer without sample were subjected to the same alignment, reconstruction, and classification procedures as in A–E. A random subset of class averages derived from classification of the buffer images after completing the same number of refinement cycles. The buffer-only images do not produce the same structure. Alignment of the buffer-only images to two additional starting references produced similar results. (G–I) A side view (G) of the reconstruction of the Tob55 dimer and a view of the dimer as seen from the cytoplasm (H). Two copies of the molecular homology model of Tob55 fitted into the density using CHIMERA. The asterisks in G–I mark density outside the β-barrel not accounted for by the Tob55 model. (I) TOB complex reconstruction from His_9-Tob55 from Fig. 7 aligned to one half of the dimer. This reconstruction is superimposed over the two molecular homology models of Tob55 that were fit to the dimer. The black arrows indicate density contributed to the complex by the association of the Tob37 subunit. This suggests that only a Tob55 monomer can bind Tob37 consistent with the stoichiometry for the complex of 1:1:1 (Tob55/Tob37/Tob38).

A list of image-processing scripts is available as a .txt file.